Journal of Fluorescence, Vol. 8, No. 1, 1998

Electronic Deactivation and Energy Transfer in Doped Oligophenylenevinylene Nanoparticles

J. Gierschner,[1] H.-J. Egelhaaf,[1] D. Oelkrug,[1,3] and K. Müllen[2]

Received October 27, 1997; accepted March 8, 1998

Suspensions of oligophenylenevinylene (nPV) nanoparticles with $n = 2$ vinylene units are doped with nPVs of longer chainlengths, $n = 3$–5. Absorption and fluorescence spectroscopy and steady-state and time-resolved fluorescence anisotropy measurements are used to determine the photophysical properties of the suspensions. Undoped nanoparticles form highly oriented H-aggregates with low fluorescence quantum yields ($\Phi_F \approx 0.1$). Introduction of bulky substituents into the particle constituting molecules perturbs the intermolecular orientation. Upon doping, efficient energy transfer to the dopants is found, changing the color and leading to enhancement of the fluorescence quantum yields up to $\Phi_F = 0.6$. The intermolecular orientation is not changed upon doping.

KEY WORDS: Oligo(phenylenevinylene) films; nanoparticles; energy transfer; time-resolved fluorescence anisotropy.

INTRODUCTION

Thin films of polyphenylenevinylenes are extensively studied for applications in electroluminescent devices [1–17]. The color and brightness of the devices are controlled by the lowest energetic singlet excitons localized at polymer domains with the longest effective conjugation lengths and the efficiencies of population and radiative deactivation of these domains. The photoluminescence quantum yield of the unmodified polymer is low ($\Phi_F = 0.04$–0.08 [3] because of interchain coupling, which favors nonradiative decay. However, the luminescence yield can be significantly enhanced, to $\Phi_F = 0.3$–0.6, by space-consuming alkyl substituents, which reduce interchain coupling, or by polar substituents, which change the intermolecular orientation from H-aggregates with forbidden luminescence emission to J-aggregates with allowed emission [2,18–20].

In this paper we investigate the color changes and intensity enhancements of phenylenevinylene luminescence by introducing emitting trap states in between the HOMO–LUMO energy gap of the host material. Instead of films we prepare suspensions of nanoparticles with diameter $d = 50$–200 nm as materials of investigation. Compared to films, these materials can be more easily doped with guest molecules in a wide range of well-defined mole fractions $x = 10^{-6}$–10^{-3}, luminescence spectra and quantum yields can be measured with standard techniques without corrections for internal reflection and anisotropic spatial emission characteristics, and absorption spectra represent the average of all domain orientations. On the other hand, no information on the anisotropy of optical constants with respect to a macroscopic surface plane is available, the contribution of surface states is more pronounced, and it is still a matter of debate whether the spectroscopic properties of nanoparticles are representative not only of microcrystalline but also of amorphous films.

[1] Institut für Physikalische und Theoretische Chemie, Universität Tübingen, Auf der Morgenstelle 8, D-72076 Tübingen, Germany.
[2] Max-Planck-Institut für Polymerforschung, Ackermannweg 10, D-55128 Mainz, Germany.
[3] To whom correspondence should be addressed.

1053-0509/98/0300-0037$15.00/0

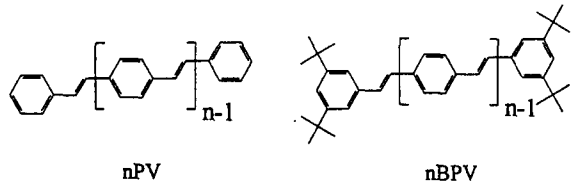

Fig. 1. Structural formulae of oligophenylenevinylenes.

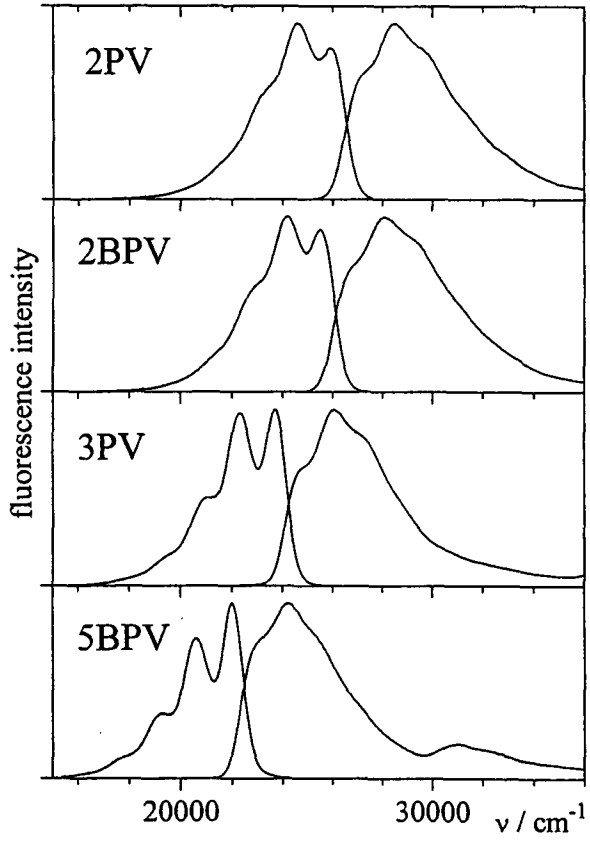

Fig. 2. Fluorescence emission and fluorescence excitation spectra of oligophenylenevinylenes in methanol (2PV, 2BPV) or dioxane (3PV, 5BPV) solution.

EXPERIMENTAL

Materials

Host materials were oligophenylenevinylenes (nPVs) with n = 2 vinylene units and nBPV with terminal t-butyl substituents (Fig. 1). The nBPVs were prepared as described elsewhere [21]. Nanoparticles (diameter, 50–200 nm) were precipitated from methanol/H_2O mixtures and measured in suspension. Nanoparticles, doped with nPV and nBPV of longer chain lengths, n = 3–5, were prepared in the same way, using mixed solutions of 2PV or 2BPV and the dopant, with mole fractions in the range of $x = 10^{-6}$–10^{-3}.

Measurements

Absorption spectra were recorded on a Perkin–Elmer Lambda-2 UV/Vis–spectrometer and fluorescence spectra on a Spex-Fluorolog 222 and a closed-cycle He cryostat. Fluorescence anisotropies were recorded with additional Glan–Thompson polarizers, and time-resolved depolarization and fluorescence decay curves were measured at the Center for Fluorescence Spectroscopy, University of Maryland, Baltimore, with the time-correlated single-photon counting technique using an argon ion laser/dye laser/frequency doubler system with 7-ps pulses and a microchannel plate detector with a 60-ps response time. The sizes of nanoparticles were determined by dynamic light-scattering measurements.

Average fluorescence decay times $\bar{\tau}$ were obtained by averaging bi- or triexponential fits using $\bar{\tau} = (\Sigma A_i\tau_i^2)/(\Sigma A_i\tau_i)$ with decay components τ_i and amplitudes A_i.

RESULTS AND DISCUSSION

Undoped 2PV and 2BPV Nanoparticles

Figure 2 presents fluorescence and $S_0 \rightarrow S_1$ absorption spectra of the hosts 2PV and 2BPV and the guests 3PV and 5BPV in dilute solutions. After the addition of water, suspensions of nanoparticles with new spectra are obtained. The main spectral properties of undoped 2PV and 2BPV nanoparticles have already been described [22–24].

The lowest energetic absorption peak A_1 of 2PV particles is very weak and redshifted against the S_{00} peak in solution by $\Delta\tilde{\nu}$ = 1600 cm^{-1} (see Table 1 and Fig. 6). On the other hand, the main absorption peak A_{max} is blueshifted against the highest vibronic peak in solution by $\Delta\tilde{\nu}$ = 5000 cm^{-1}. This spectral shape is typical of H-aggregates, where the electronic transition dipoles of adjacent molecules are aligned in parallel side by side, making transitions to the low energetic A_1 wing of the molecular exciton band forbidden or only weakly allowed [25]. As a consequence, also, the highest energetic fluorescence peak F_1 is weak, and intensity is gained mainly by coupling with asymmetric valence vibrations of the carbon skeleton, yielding F_{max} and a consecutive totally symmetric progression of $\tilde{\nu}$ = 1370 cm^{-1} (see Fig. 5a). The fluorescence quantum efficiency decreases from Φ_F = 0.9 in solution to Φ_F = 0.08–0.13

Table I. Fluorescence and Absorption Maxima of Oligophenylenevinylenes in Solution and Nanoparticles

	Fluorescence maxima $\tilde{\nu}$ (cm^{-1})			Absorption maxima $\tilde{\nu}$ (cm^{-1})		
	F_{max}	F_1	S_{00}	S_{00}	A_1	A_{max}
nPVs in solution[a]						
2PV			25,800	27,050		
2BPV			25,500	26,650		
3PV			23,700	24,700		
5BPV			22,050	23,050		
Nanoparticles (hosts)						
2PV	22,750	24,050			25,400	~34,000
2BPV	23,350	24,800			26,000	~29,300
Nonoparticles (guests)						
3PV (in 2PV)			22,400	—[b]		
5BPV (in 2PV)			20,900	22,000		
5BPV (in 2BPV)			21,800	23,000		

[a]2PV and 2BPV in methanol; 3PV and 5BPV in dioxane.
[b]S_{00} transition obscured by host absorption.

in the particles, depending somewhat on the precipitation conditions. The fluorescence decay time behaves oppositely and increases from τ = 1.2 ns in solution to an average of $\bar{\tau}$ = 2–3 ns with a slightly nonexponential decay characteristics (see Table II). Upon cooling to T = 50 K both the fluorescence efficiency and the decay time increase by a factor of approximately three, yielding an upper limit for the intrinsic decay time of τ_0 = 30 ns. This value is about a factor of 20 longer than in solution, in accordance with the low oscillator strength of the emitting state of H-aggregates.

The short- and long-range order of the H-aggregates can be estimated from the degree of fluorescence polarization after excitation with polarized laser pulses. Fluorescence anisotropy decay times τ_a of the nanoparticles are significantly shortened against τ_a in solution (see Figs. 3 and 4). The reason is that depolarization is not caused by rotational diffusion of the individual molecules or the whole nanoparticle (the rotational correlation time of the latter is of the order of microseconds) but by energy transfer from the originally excited molecules to neighbors with different orientations. According to Fig. 3 the fluorescence anisotropy decays with τ_a = 43 ps for 2PV and levels off at a finite value of r_∞ = 0.22, from which a maximum deviation $\theta \approx 35°$ of the emitting dipole from the originally excited dipole can be calculated [23]. The calculations are carried out inserting a value of r_0 = 0.36 for the initial anisotropy. This value is very similar to the r_0 values of isolated molecules, which were determined for 2PV and 2BPV in CH_2Cl_2 from time-resolved fluorescence anisotropy measurements (see Fig. 4).

Compared to 2PV, the spectral properties of 2BPV are much less changed upon condensation to nanoparticles. The intensities of the first absorption and fluorescence peaks, A_1 and F_1, are only slightly lowered and their positions only little shifted against the corresponding S_{00} maxima in solution (see Table I). The blueshift of A_{max} against S_{max} is reduced to $\Delta\tilde{\nu}$ = 1000 cm^{-1}. All effects can be explained by reduced intermolecular exciton coupling due to the bulky t-butyl substituents, which increase the intermolecular distances. In addition, the fluorescence anisotropy decreases to r_∞ = 0 after a very short decay period (see Fig. 3), indicating that some residual short-range order but no long-range order of parallel aligned transition dipoles is present in 2BPV nanoparticles.

Doped Nanoparticles

2PV Nanoparticles Doped with nPVs of Longer Chain Lengths

Prior to precipitation, the 2PV solutions were doped with one additional component of nPV or nBPV, n = 3–5, as well as with mixtures of them. Here we report on the results obtained with 3PV and 5BPV. At doping levels $x > 2 \cdot 10^{-5}$, new fluorescence bands of the guests appear and the total fluorescence quantum yields increase to a present maximum in the range of Φ_F = 0.6–0.7. Some fluorescence spectra of 2PV/3PV are represented in Fig. 5a, and the corresponding total as well as partial fluorescence quantum yields in Fig. 5b. With increasing x, the yield of the host decreases somewhat,

Table II. Luminescence Data of Oligophenylenevinylenes in Solution and 2PV Nanoparticles Doped with nPV and nBPV (x = Mole Fraction of Dopant): Fluorescene Quantum Yields Φ_F and Fluorescence Rise[a] and Decay Components: Bi- (Tri-)-exponential Fits, with Amplitudes in Parentheses

	Mole fraction of dopant x	Temp (K)	Fluorescence yield: Absolute Φ_F	Fluorescence yield: Relative Contrib. (%) 2PV	Fluorescence yield: Relative Contrib. (%) Dopant	Rise and decay components τ_i/ns (rel. ampl.): Host	Rise and decay components τ_i/ns (rel. ampl.): Dopant
Solution data at T = 293 K							
2PV			0.90			1.20	
3PV			0.85			1.10	
2BPV			0.86			1.10	
5BPV			0.71			0.73	
2PV nanoparticles (undoped)		293	0.10			2.1 (0.76)	
						3.8 (0.24)	
		50	—			2.3 (0.61)	
						11.6 (0.39)	
2PV nanoparticles doped with							
3PV	$2.0 \cdot 10^{-4}$	293	0.25	24	76	2.1	0.5 (−1.00)
							0.5 (0.85)
							3.1 (0.20)
	$1.2 \cdot 10^{-3}$	293	0.60	7	93	—[b]	0.7 (−1.00)
							1.9 (0.71)
							5.0 (0.38)
5BPV	$7.3 \cdot 10^{-4}$	293	0.43	10	90	1.3 (0.42)	0.6 (−1.00)
						3.5 (0.58)	4.2 (1.13)
		50	—	45	55	2.0 (0.17)	0.5 (−1.00)
						7.6 (0.83)	5.9 (1.13)
	$1.2 \cdot 10^{-3}$	293	0.50	8	92	—	0.7 (−1.00)
							1.7 (0.82)
							4.8 (0.19)

[a]Negative amplitudes of the rise components are normalized to unity.
[b]Not given because of possible contributions of guest emission.

whereas the yield of the guest strongly increases. The shape of the guest fluorescence spectrum corresponds to the spectrum of 3PV in dioxane solution (see Fig. 2), but the whole spectrum is shifted in 2PV by $\Delta\tilde{\nu} = 1300$ cm^{-1} to the red. A similar shift of $\Delta\tilde{\nu} = 1100$ cm^{-1} is found for 5BPV as guest. The main reason for the redshift is the high polarizability of the host at the low energetic wing of the first absorption band, which yields refractive indexes $n > 2.5$ into the direction of the long molecular axis. Planarization of 3PV in the rigid host lattice may be also a source for redshifted fluorescence. However, this effect seems to be important only at low temperatures, where the whole spectra of guest and host, inclusive of A_1, experience an additional redshift of $\Delta\tilde{\nu} \approx 300$ cm^{-1}. Figure 6 illustrates the effect for 2PV/5BPV, where host and guest spectra are more clearly separated than in 2PV/3PV. The fluorescence excitation spectrum is identical from $\tilde{\nu} > 24{,}000$ cm^{-1} for host H and guest G so that G^* is populated exclusively via H^*. Upon cooling, the efficiency for excitation energy transfer is considerably lowered since the H^* fluorescence increases and the G^* fluorescence decreases in intensity. Finally, Fig. 6 presents steady-state fluorescence anisotropies for H and G which are equal over the whole fluorescence band, with values of $r_F = 0.22$. Thus 5BPV must be oriented with its long axis parallel to the side-by-side arrangements of the 2PV molecules. The only difference is found in the initial part of the time-resolved anisotropy decay curve, which starts at a lower r_0 for G than for H (see Fig. 3). However, this is a reasonable difference since the nearest G is usually not very close to the primary excited H^* so that some orientational mismatch becomes operative even upon direct Förster transfer. Direct excitation of the guest at $\tilde{\nu}_{exc} \leq 23{,}000$ cm^{-1} results in r_F values close to the upper limit of 0.36 for isolated molecules (see Fig. 6). This shows that energy transfer from the luminescent guests to molecules with different orientations is negligible. It

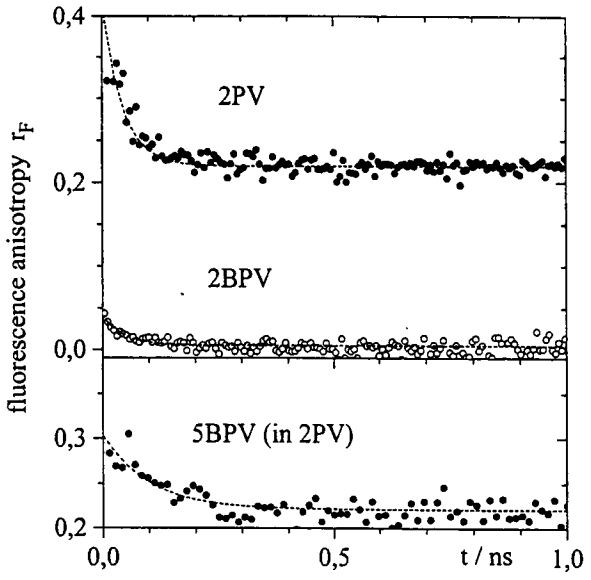

Fig. 3. Time-resolved fluorescence anisotropies r_F of 2PV and 2BPV nanoparticles (upper scale) and 5BPV in 2PV (x = 1.2·10^{-3}, lower scale) upon pulse excitation (Δt = 7 ps, $\tilde{\nu}_{exc}$ = 27,800 cm^{-1}, and $\tilde{\nu}_{em}$ ≤ 25,700 cm^{-1} for 2PV and 2BPV, $\tilde{\nu}_{em}$ ≤ 18,200 cm^{-1} for 5BPV in 2PV). Dashed lines are exponential fits with τ = 43 ps, r_∞ = 0.22, for 2PV, τ = 80 ps, r_∞ = 0, for 2BPV and τ = 100 ps, r_∞ = 0.22, for 5BPV in 2PV.

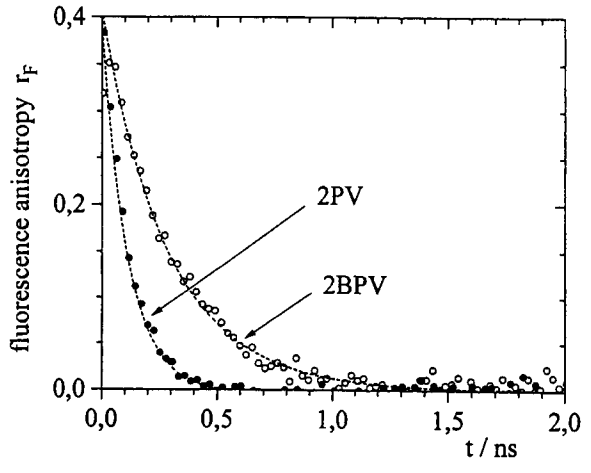

Fig. 4. Time-resolved fluorescence anisotropies r_F of 2PV (filled circles) and 2BPV (open circles) in CH_2Cl_2 upon pulse excitation (Δt = 7 ps, $\tilde{\nu}_{exc}$ = 27,800 cm^{-1}, and $\tilde{\nu}_{em}$ ≤ 25,700 cm^{-1}). Dashed lines are exponential fits with τ = 114 ps, r_∞ = 0, for 2PV and τ = 290 ps, r_∞ = 0, for 2BPV.

also proves that rotational depolarization due to the motion of the nanoparticles plays no role on the nanosecond time scale.

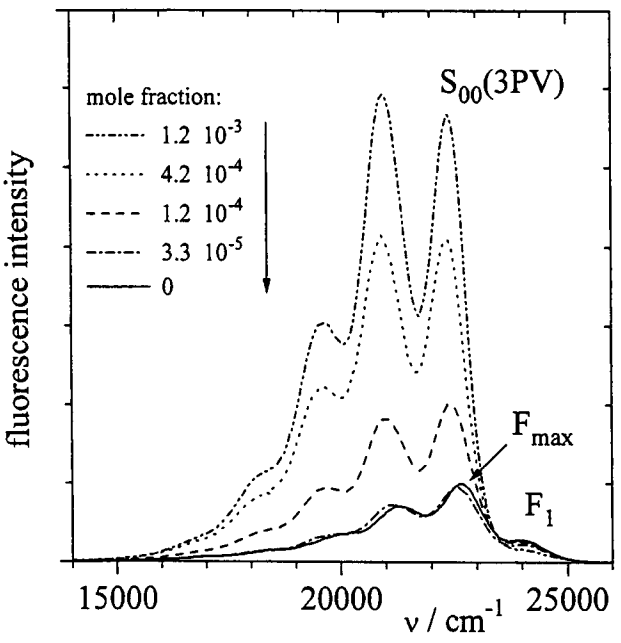

Fig. 5a. Fluorescence emision spectra of 2PV nanoparticles doped with different mole fractions x of 3PV.

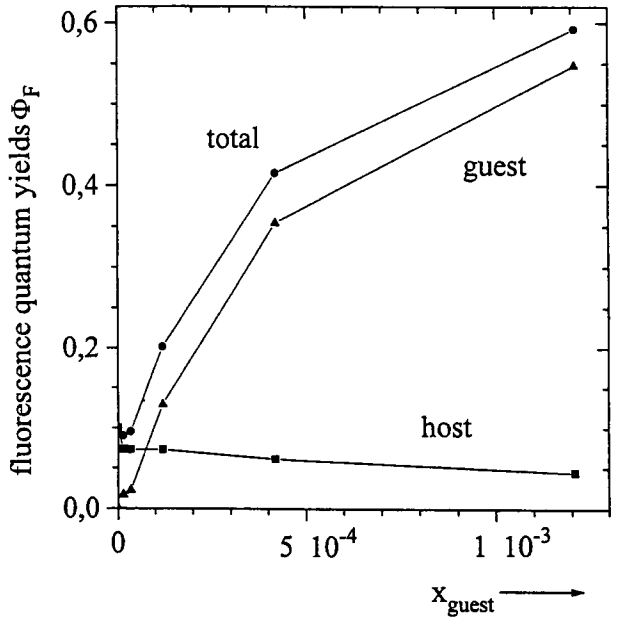

Fig. 5b. Fluorescence quantum yields Φ_F of the host (2PV) and guest (3PV) as well as their sum (total) versus the mole fraction of the guest.

2BPV Nanoparticles Doped with nPVs

Figure 7 presents fluorescence emission and excitation spectra of 2BPV nanoparticles, doped with 5BPV

at a mole fraction $x = 1.1 \cdot 10^{-3}$. The fluorescence spectrum of undoped nanoparticles is represented for comparison. In comparison to 2PV nanoparticles, the effect of doping on the photophysical properties is much less pronounced. The total fluorescence quantum yield increases by only a factor of 1.4 (instead of the factor of 6 in Fig. 5a). Also, the decrease in the host fluorescence is weak. These effects are ascribed to less efficient energy transfer, due to larger intermolecular distances caused by the bulky t-butyl substituents. Furthermore, the redshift of guest fluorescence compared to solution is only $\Delta\tilde{\nu} = 200$ cm^{-1}. This is much lower than in 2PV, due to the lower effective refractive index of the disordered host. The steady-state fluorescence is completely depolarized over the 2BPV and 5BPV spectra (see Fig. 7), indicating complete disorder, with the exception of directed excited 5BPV guests ($\tilde{\nu}_{exc}$ = 22,000–24,000 cm^{-1}), where the fluorescence rises to $r_F \approx 0.36$ because no depolarizing energy transfer is now possible.

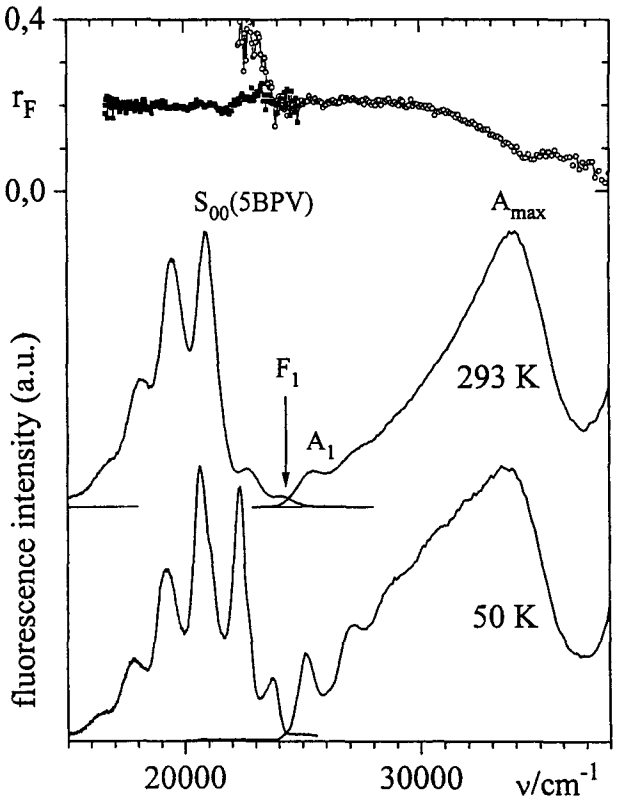

Fig. 6. Fluorescence and fluorescence excitation spectra of 2PV nanoparticles, doped with 5BPV ($x = 4.5 \cdot 10^{-4}$) at T = 293 and 50 K. Steady-state anisotropies r_F at T = 293 K are presented as filled squares for $\tilde{\nu}_{exc}$ = 31,300 cm^{-1} and as open circles for $\tilde{\nu}_{em}$ = 17,500 cm^{-1}.

Excited-State Deactivation and Energy Transfer

The results of time-resolved fluorescence experiments are very similar for all 2PV/guest systems described in this paper. The emitting state F_1 of H is populated within $\tau < 10$ ps, i.e., faster than the time resolution of our apparatus. The decay curve is nonexponential, with an average decay time of $\bar{\tau}_H$ = 2–2.5 ns (average of bi- or triexponential fits). The value of $\bar{\tau}_H$ is somewhat smaller than in undoped 2PV, but no systematic reduction of $\bar{\tau}_H$ with increasing x can be observed. The main reduction is found already for very low doping levels of $x < 3 \cdot 10^{-5}$, then $\bar{\tau}_H$ remains more or less constant. The emitting state of G *is* populated with a clear rise component (see Fig. 8) in the order of $\tau_{r,G}$ = 0.5 ns and is deactivated nonexponentially with $\bar{\tau}_{d,G}$ = 2.5–3.5 ns, i.e., with decay kinetics similar to that of the host. However, the long decay component of G is somewhat longer than that of H. At low temperatures, the rise time of G remains almost unchanged, whereas the average decay times of H and G increase to $\bar{\tau}_H \approx \bar{\tau}_{d,G} \approx$ 6–7 ns. Again, the decay times of H and G are similar but not equal, the long decay component of G now being shorter than that of H.

A simple explanation for the long decay times of G, which are longer by a factor of 5–8 than upon direct excitation in dilute solution, (see Table II) can be given by the consecutive reaction $H^* + G \rightarrow H + G^* \rightarrow H + G + h\nu_G$, where the first step incorporates energy migration via neighboring host molecules as well as long-range Förster transfer. Since the lifetime of H^* is distinctly longer than that of directly excited G^* in solution, the decay of G^* intensity is determined in the consecutive reaction by the population step, and the rise of G^* intensity by the deactivation step. However, proof can be given only when the photophysics of G has been investigated in nanoparticles also upon direct excitation.

Unfortunately, the simple model of a linear consecutive reaction is not consistent with the results of fluorescence quantum yields. The main decrease in τ_H and $\Phi_{F,H}$ of the host takes place already at very low x, whereas $\Phi_{F,G}$ increases only weakly. At higher x, both τ_H and $\Phi_{F,H}$ decrease only weakly, whereas $\Phi_{F,G}$ increases strongly. Thus, over the main range of x, the emitting F_1 state of H cannot be the source for G^*. The latter must be populated at the expense of the nonradiative channel of undoped H^*, without affecting the majority of F_1. It is difficult to establish such a mechanism in a homogeneous system, but it is also not known whether G is homogeneously distributed in the nanoparticle. A possible distribution could be as follows: only a very small portion of G is homogeneously dis-

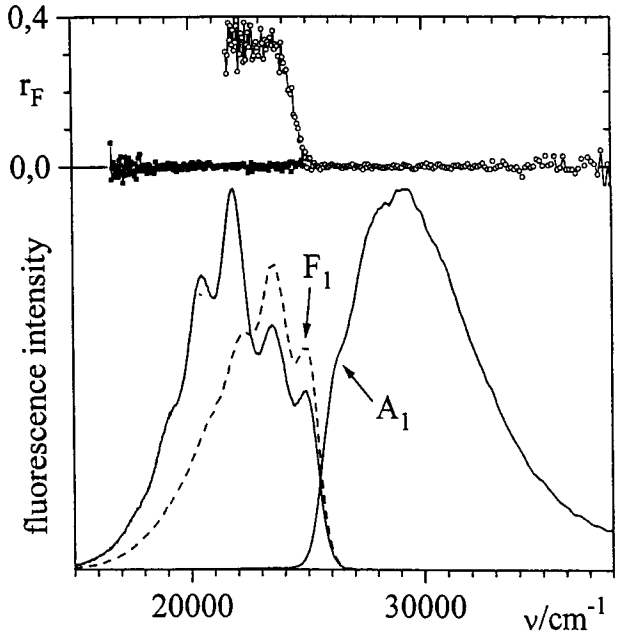

Fig. 7. Fluorescence and fluorescence excitation spectra of 2BPV nanoparticles, doped with 5BPV (x = 1.1·10^{-3}). Stationary fluorescence anisotropies r_F are presented as filled squares for $\tilde{\nu}_{exc}$ = 31,300 cm^{-1} and as open circles for $\tilde{\nu}_{em}$ = 17,500 cm^{-1}. Dashed line: Fluorescence spectrum of undoped 2BPV nanoparticles.

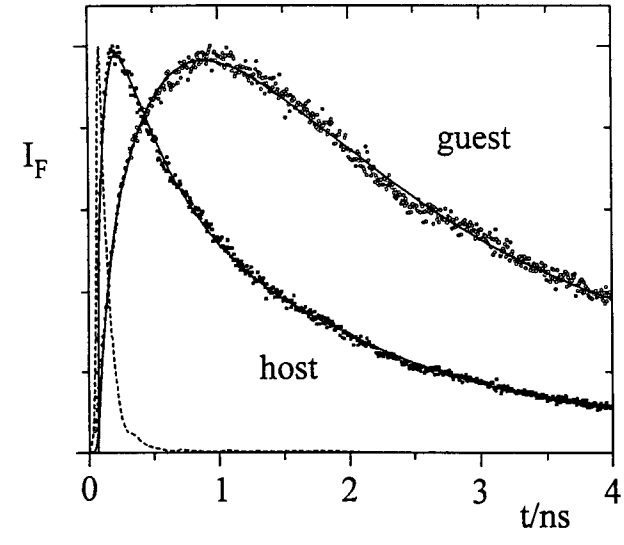

Fig. 8. Initial part of time-resolved fluorescence of 2PV nanoparticles doped with 3PV (x = 2·10^{-4}). Dashed line: laser pulse.

solved in the particle, and the rest segregates close to the periphery. The dissolved part acts as a luminescence quencher via polaron pair formation, $H^* + G \rightarrow H^+ + G^-$, and is responsible for the initial decrease in τ_H and $\Phi_{F,H}$. The segregated part competes with quenching centers at the periphery and is responsible for the strong increase in the guest fluorescence without affecting the main part of F_1.

CONCLUSIONS

Nanoparticles of unsubstituted nPVs form systems with molecules oriented in parallel, side by side. Due to H-aggregation, fluorescence quantum yields are significantly reduced compared to those in solution. Introduction of bulky substituents into the particle constituting molecules reduces the parallel intermolecular orientation.

Doping 2PV particles with nPVs of longer chain lengths at mole fractions $x \leq 10^{-3}$ gives us the opportunity to tune the color and increase the fluorescence quantum yield up to Φ_F = 0.6. The intermolecular orientation is not influenced upon doping. Emission spectra of the guests are strongly redshifted against solution, due to high refractive indexes of the host.

Doping of 2BPV nanoparticles causes less efficient energy transfer to the guest, due to larger intermolecular distances.

ACKNOWLEDGMENTS

We thank U. Stalmach (University of Mainz) for preparing 3PV. Time-resolved fluorescence was done at the Center for Fluorescence Spectroscopy, University of Maryland, Baltimore. We thank J. R. Lakowicz for giving us the opportunity to use these facilities and H. Malak for scientific and technical assistance.

REFERENCES

1. J. H. Burroughes, D. D. C. Bradley, A. R. Brown, R. N. Marks, K. Mackey, R. H. Friend, P. L. Burn, and A. B. Holmes (1990) *Nature* **347**, 539–541.
2. I. D. W. Samuel, G. Rumbles, C. J. Collison, B. Crystall, S. C. Moratti, and A. B. Holmes (1996) *Synth. Met.* **76**, 15–18.
3. G. Köpping-Grem, G. Leising, M. Schimetta, F. Stelzer, and A. Huber (1996) *Synth. Met.* **76**, 53–56.
4. M. G. Harrison, J. Grüner, and G. C. W. Spencer (1996) *Synth. Met.* **76**, 71–75.
5. J. Cornil, D. Beljonne, D. A. dos Santos, and J. L. Brédas (1996) *Synth. Met.* **76**, 101–104.
6. M. Herold, J. Gmeiner, W. Rieß, and M. Schwoerer (1996) *Synth. Met.* **76**, 109–112.
7. F. Meghadi, G. Leising, W. Fischer, and F. Stelzer (1996), *Synth. Met.* **76**, 113–115.
8. V. Cimarová and D. Neher (1996) *Synth. Met.* **76**, 125–128.

9. D. G. Lidzey, M. S. Weaver, T. A. Fisher, M. A. Pate, D. M. Whittaker, M. S. Skolnick, and D. D. C. Bradley (1996) *Synth. Met.* **76**, 129–132.
10. J. Grüner, F. Cacialli, I. D. W. Samuel, and R. H. Friend (1996) *Synth. Met.* **76**, 137–140.
11. F. Cacialli, R. N. Marks, R. H. Friend, R. Zamboni, C. Taliani, S. C. Moratti, and A. B. Holmes (1996) *Synth. Met.* **76**, 145–148.
12. D. R. Baigent, P. G. May, and R. H. Friend (1996) *Synth. Met.* **76**, 149–152.
13. A. C. Grimsdale, F. Cacialli, J. Grüner, X.-C. Li, A. B. Holmes, S. C. Moratti, and R. H. Friend (1996) *Synth. Met.* **76**, 165–167.
14. R. H. Friend, G. J. Denton, J. J. M. Halls, N. T. Harrison, A. B. Holmes, A. Köhler, A. Lux, S. C. Moratti, K. Pichler, N. Tessler, and K. Towns (1997) *Synth. Met.* **84**, 463–470.
15. I. D. Samuel, G. Rumbles, C. J. Collison, R. H. Friend, S. C. Moratti, and A. B. Holmes (1997) *Synth. Met.* **84**, 497–500.
16. R. E. Gill, A. Hiberer, P. F. van Hutten, G. Berentschot, M. P. L. Werts, A. Meetsma, J.-C. Wittmann, and G. Hadziioannou (1997) *Synth. Met.* **84**, 637–638.
17. M. Hohloch, J. L. Segura, S. E. Döttinger, D. Hohnholz, E. Steinhuber, H. Spreitzer, and M. Hanack (1997) *Synth. Met.* **84**, 319–322.
18. D. D. C. Bradley (1997) in *Proc. Symp. M, E-MRS*, 1997 Spring Meeting, Strasbourg (in press).
19. D. Oelkrug, A. Tompert, H.-J. Egelhaaf, M. Hanack, E. Steinhuber, M. Hohloch, H. Meier, and U. Stalmach (1996) *Synth. Met.* **83**, 231–237.
20. D. Oelkrug, A. Tompert, J. Gierschner, H.-J. Egelhaaf, M. Hanack, M. Hohloch, and E. Steinhuber (1997) *Proc. SPIE* **3145**, 242–253.
21. R. Schenk, H. Gregorius, K. Meerholz, J. Heinze, and K. Müllen (1991) *J. Am. Chem. Soc.* **113**, 2634–2647.
22. D. Oelkrug, H.-J. Egelhaaf, J. Gierschner, and A. Tompert (1996) *Synth. Met.* **76**, 249–253.
23. H.-J. Egelhaaf, J. Gierschner, and D. Oelkrug (1996) *Synth. Met.* **83**, 221–226.
24. J. Gierschner, H.-J. Egelhaaf, and D. Oelkrug (1997) *Synth. Met.* **84**, 529–530.
25. R. M. Hochstrasser and M. Kasha (1964) *Photochem. Photobiol.* **3**, 317–331.